

HESS J1832–085: evidence for a new gamma-ray binary candidate

Agnibha De Sarkar¹ and Tanuman Ghosh²

¹ Institute of Space Sciences (ICE, CSIC), Campus UAB, Carrer de Can Magrans s/n, 08193 Barcelona, Spain
e-mail: desarkar@ice.csic.es

² Inter-University Centre for Astronomy and Astrophysics, Post Bag 4, Ganeshkhind, Pune 411007, India

Received XXXX; accepted YYYY

ABSTRACT

Context. The Galactic plane survey conducted by the High Energy Stereoscopic System (H.E.S.S.) has revealed numerous teraelectronvolt (TeV) sources, many of which remain unidentified. HESS J1832–085 is a point-like TeV source lacking a confirmed multiwavelength (MWL) counterpart. In this paper, we present evidence that HESS J1832–085 is likely a gamma-ray binary.

Aims. We aim to investigate the nature of HESS J1832–085 using *Fermi*-LAT and X-ray data, complemented by broadband radiative modeling, to assess its classification as a potential gamma-ray binary.

Methods. We analyzed ~ 17.3 yr of *Fermi*-LAT data between 0.1 and 500 GeV to establish the gigaelectronvolt (GeV) counterpart of HESS J1832–085, including performing spectral, spatial, and periodicity analyses. Archival X-ray observations were examined to search for a counterpart and to characterize its spectrum and potential variability. The broadband emission was interpreted using models commonly applied to gamma-ray binaries.

Results. We detect a point-like GeV gamma-ray source spatially consistent with HESS J1832–085, with spectral properties compatible with known gamma-ray binaries. No significant GeV periodic modulation is detected. A potential X-ray counterpart is identified in archival X-ray data, exhibiting a hard, absorbed spectrum and moderate variability. The broadband spectral energy distribution is reproduced by the adopted binary radiative model.

Conclusions. Our results indicate that HESS J1832–085 is likely a gamma-ray binary candidate, motivating dedicated MWL follow-up observations to confirm the source nature.

Key words. binaries: general – Gamma rays: general – X-rays: binaries – Stars: individual: HESS J1832–085

1. Introduction

Gamma-ray binaries are rare high-energy (HE) systems (Dubus 2013) consisting of a compact object, typically a neutron star, orbiting an O- or Be-type companion. In pulsar-powered systems, the relativistic pulsar wind collides with the stellar wind, forming a shock where particles can be efficiently accelerated, likely via diffusive shock acceleration (Maraschi & Treves 1981; Dubus 2006; Bogovalov et al. 2008; Bosch-Ramon et al. 2012; Dubus 2013; Sironi & Spitkovsky 2011; Huber et al. 2021). The resulting relativistic particles produce non-thermal emission through various radiative processes. Alternative emission scenarios may arise depending on the nature of the compact object, the companion star, and the system geometry (Romero et al. 2003; Bosch-Ramon & Paredes 2004; Aharonian et al. 2005; Lyne et al. 2015). Confirmed and candidate gamma-ray binaries are generally characterized by soft teraelectronvolt (TeV) spectra and hard, strongly absorbed X-ray emission.

HESS J1832–085 is a point-like ($\sim 0.02^\circ \pm 0.012^\circ$) TeV source discovered in the Galactic plane survey by the High Energy Stereoscopic System (H.E.S.S.) (H. E. S. S. Collaboration 2018) at Galactic longitude $l = 23.21^\circ$ and latitude $b = 0.29^\circ$. A radio pulsar PSR J1832–0827 (Clifton & Lyne 1986) at a distance 4.4–6.1 kpc (Frail et al. 1991; Cordes & Lazio 2002), with a spin-down luminosity $\dot{E} = 9.3 \times 10^{33}$ erg s⁻¹ (Hobbs et al. 2004), braking index $n = 2.5 \pm 0.9$ (Johnston & Galloway 1999) and a characteristic age $\tau_c \approx 200$ kyr was detected to be spatially coincident with the H.E.S.S. source. Additionally, another millisecond pulsar, PSR J1832–0836 at a distance of 1.1 kpc, with

a 2.7 ms period (Burgay et al. 2013), $\dot{E} = 1.7 \times 10^{34}$ erg s⁻¹, and $\tau_c = 5 \times 10^9$ yr was also detected in the region (Cordes & Lazio 2002). Notably, a supernova remnant (SNR) G23.11+0.18, detected in radio, was found to be spatially consistent with the H.E.S.S. source, at a distance of 4.6 ± 0.8 kpc. (Maxted et al. 2019). AX J1832.3–0840, most likely an intermediate polar (IP) (Kaur et al. 2010), and a steep-spectrum radio point source (Maxted et al. 2019), both of which are unlikely to be associated with the H.E.S.S. source, are also present in the region. Additionally, a highly absorbed and hard spectrum X-ray source was found near the centroid of HESS J1832–085 from the analysis of *Suzaku* data (Aktekin 2025). The X-ray source was interpreted as a possible pulsar wind nebula; however, not without its demerits (Aktekin 2025). Fig. 1 shows the significance map of the region around HESS J1832–085, with all the spatially consistent sources marked on it.

2. Results

2.1. GeV counterpart of HESS J1832–085

The details of *Fermi*-LAT analysis are given in Appendix A. The analysis revealed a possible gigaelectronvolt (GeV) counterpart of the H.E.S.S. source, 4FGL J1832.4–0847, at $l = 23.0091^\circ \pm 0.0137^\circ$ and $b = 0.1816 \pm 0.0128$, at an offset of 0.23° , and with a detection significance of $\sim 15\sigma$. The spectrum of the 4FGL source can be best described by a log-parabola function, given by $dN/dE \propto (E/E_b)^{-\alpha_{LP}-\beta_{LP} \log(E/E_b)}$, where the best-fit spectral parameters are given by $\alpha_{LP} = 2.01 \pm 0.01$, $\beta_{LP} = 0.647 \pm 0.006$, and

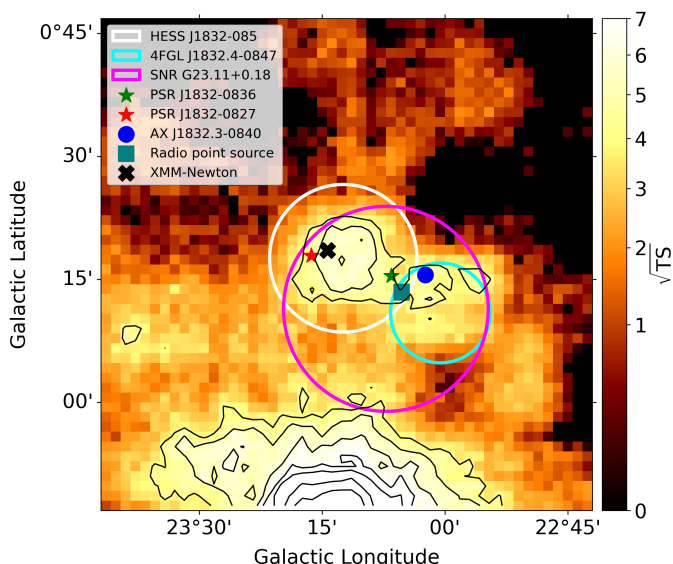


Fig. 1: H.E.S.S. significance map of the region centered at HESS J1832–085. The colorbar signifies the \sqrt{TS} value of the region. The white circle denotes the spectral extraction region of HESS J1832–085. The cyan and magenta circles signify the GeV counterpart 4FGL J1832.4–0847 and SNR G23.11+0.18. The radio pulsar PSR J1832–0827 and millisecond pulsar PSR J1832–0836 are shown as red and green stars. The blue circle denotes the intermediate polar AX J1832.3–0840, and the teal square marks the radio point source in the region. The *XMM-Newton* detected X-ray source is shown with a black cross.

E_b is the scale energy fixed at 2.56 GeV. The integrated energy flux of 4FGL J1832.4–0847 between 0.1 to 500 GeV was found to be $(1.497 \pm 0.117) \times 10^{-11}$ erg cm $^{-2}$ s $^{-1}$. We also checked the source extension using a *RadialDisk* model, and found a best-fit extension of $0.1014^{+0.0231}_{-0.0262}$ deg, with $TS_{\text{ext}} = 2.379$ ($\sim 1.5\sigma$). The extension test statistic, defined as $TS_{\text{ext}} = 2 \log(\mathcal{L}_{\text{ext}}/\mathcal{L}_{\text{ps}})$ comparing extended and point-source hypotheses, is below the 5σ threshold, indicating that the detected 4FGL source is consistent with a point-like origin. Other than the *Fermi* orbit precession period of ~ 53 days, no other periodicity was unambiguously detected. Although a peak at ~ 115 days for the unweighted light curve and a peak at ~ 206 days for the weighted light curve were detected to exceed the 5% significance level, these detections are not robust to the variations in the model. Therefore, we refrain from claiming a possible detection of orbital periodicity from our analysis at this point.

2.2. X-ray counterpart of HESS J1832–085

The X-ray counterpart of HESS J1832–085 has been investigated with *Suzaku* data by Aktekin 2025. Here, we further study archival data from *XMM-Newton*, *Chandra*, and *Swift* to explore the source’s spectrum and long-term flux variability. The data extraction and analysis methodology is standard, using SAS v22.1.0 for *XMM-Newton*, HEASOFT v6.35.1 for *Swift*, and CIAO v4.15 for *Chandra* (See details in the Appendix B). The *Chandra* and *Swift* data are utilized only for the study of long-term flux variation, and the *XMM-Newton* data are used for detailed spectral analysis and further for the multiwavelength (MWL) spectral energy distribution (SED) modeling.

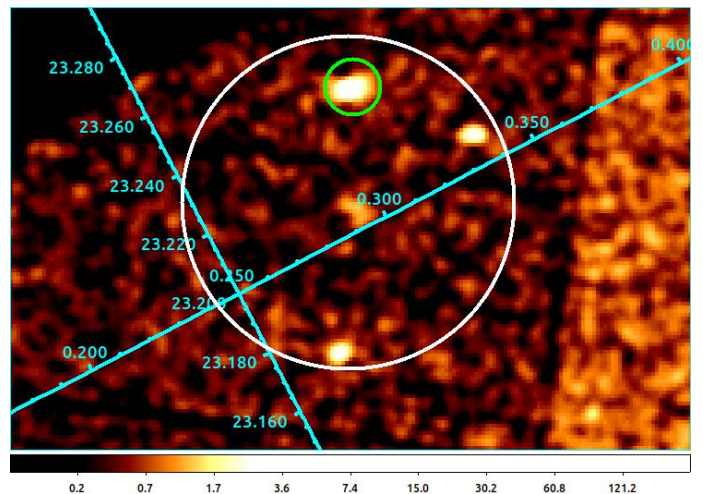


Fig. 2: *XMM-Newton* MOS2 image depicting the source region with a circle of 30'' in green ($l = 23.2390621^\circ$, $b = 0.3090542^\circ$). This coordinate is close to the analysis of Aktekin (2025) with much better constraint owing to a better spatial resolution of *XMM-Newton* detectors compared to that of *Suzaku*. The white circle, denoting the 95% positional uncertainty, is centered on HESS J1832–085 centroid (H. E. S. S. Collaboration 2018) and has a radius of 0.05°. The image is smoothed with a Gaussian kernel for visual purposes.

We show the *XMM-Newton* image as a representation to portray the source location in Fig. 2. We can see that within the 95% positional uncertainty circle of the H.E.S.S. source, the source we marked with a green circle is the brightest and also identified as the X-ray counterpart of the H.E.S.S. source by Aktekin (2025). Thus, we investigate further to establish a plausible relation between this source and HESS J1832–085.

Analysis of *XMM-Newton* data shows that the source is spectrally hard and is well fitted with a simple absorbed power-law model (see Fig. 3). Interestingly, the neutral absorption parameter, from model *tbabs* with relevant elemental abundances (Wilms et al. 2000) and absorption cross-section (Verner et al. 1996), is high, i.e., $N_{\text{H}} = 8.0^{+2.5}_{-2.0} \times 10^{22}$ cm $^{-2}$, thereby indicating strong absorption. The best-fitted power-law index is $\Gamma = 1.2^{+0.5}_{-0.4}$, and the unabsorbed flux in 2.0–10.0 keV band is $1.2^{+0.2}_{-0.1} \times 10^{-12}$ erg s $^{-1}$ cm $^{-2}$.

In Fig. 4, we show the long-term unabsorbed 2.0–10.0 keV flux variation over time, which shows a moderate variability. We have fitted the *XMM-Newton*, *Chandra*, *Swift* spectra with a simple absorbed power-law and estimated the flux. For *Suzaku*, we have obtained the flux value from Aktekin 2025.

3. Discussion

In this section, we discuss whether the spectral properties of HESS J1832–085 support its classification as a candidate gamma-ray binary. The X-ray spectrum, derived from the *XMM-Newton* observation, is hard, strongly absorbed, and non-thermal. The hard spectral slope is compatible with those commonly measured in established gamma-ray binaries (see, for e.g., Hinton et al. 2009; Eger et al. 2016). The system is also strongly absorbed, and the column density obtained from *XMM-Newton* analysis is very much consistent with that obtained for the X-ray counterpart of HESS J1832–093 (Eger et al. 2016; Martí-Devesa & Reimer 2020). The log-parabolic spectral shape

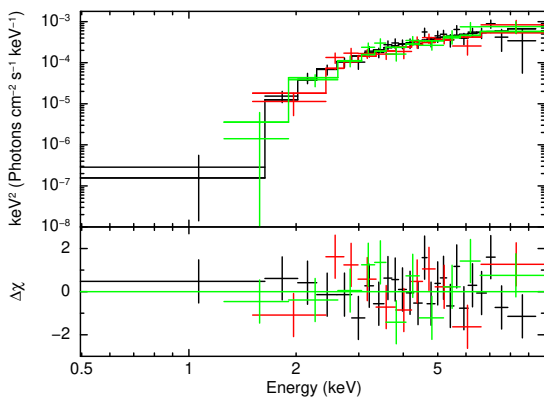


Fig. 3: The spectra and residual of the source with a simple absorbed power-law fit to the *XMM-Newton* observation. pn, MOS1, and MOS2 are depicted with black, red, and green, respectively. Spectra are rebinned for visual purposes.

of the GeV counterpart 4FGL J1832.4–0847 is also similar to that of HESS J1832–093 (Martí-Devesa & Reimer 2020).

A defining feature of a confirmed gamma-ray binary would be the presence of orbital modulation, particularly in X-ray band, whereas the same in the GeV band is difficult to attain (Tam et al. 2020; De Sarkar et al. 2022). In the case of HESS J1832–085, no significant GeV orbital periodicity is detected from the analysis of *Fermi*-LAT data, as discussed above. This non-detection does not necessarily argue against a binary scenario, as orbital modulation in GeV can be weak, and difficult to detect depending on the orbital inclination, eccentricity, viewing geometry, or limited photon statistics. From standard aperture photometry analysis, as the one discussed here, it is hard to detect a GeV orbital periodicity from a blind search. Nevertheless, the long-term light curve produced from available X-ray data (see Fig. 4) hints towards a flux variability, which is qualitatively similar to the behavior observed in other gamma-ray binary systems (see Fig. 4 of Eger et al. 2016). Long-term monitoring of the source is therefore essential, especially regular X-ray observations with *Swift* or comparable facilities would provide the probe for orbital periodicity, given the typically stronger modulation observed in X-ray. If an orbital periodicity is obtained from future X-ray analysis, that information can be used to probe the same in GeV band via a more detailed epoch folding method employed by Martí-Devesa & Reimer (2020).

The broadband SED of HESS J1832–085 is shown in Fig. 5. From the plot, it can be seen that the GeV and X-ray spectra of the respective counterparts show remarkable similarity with those of the established gamma-ray binaries. Specifically, a hard, strongly absorbed spectrum is observed in X-ray, whereas a softer spectrum ($\Gamma = 2.38 \pm 0.14$) is observed in TeV range (H. E. S. S. Collaboration 2018), typical of gamma-ray binaries. We further try to explain the broadband SED by solving the one-zone diffusion-loss equation using *GAMERA* (Hahn 2015; Hahn et al. 2022), considering a single leptonic population, assumed to be accelerated at the intrabinary shock. Note that at radio frequencies, no counterpart is detected at the *XMM-Newton* position, and the NVSS upper limit (Condon et al. 1998) constrains the minimum energy of the lepton population. The simple modeling discussed here is illustrative, and follows similar arguments in Hinton et al. (2009). Accelerated electrons are assumed

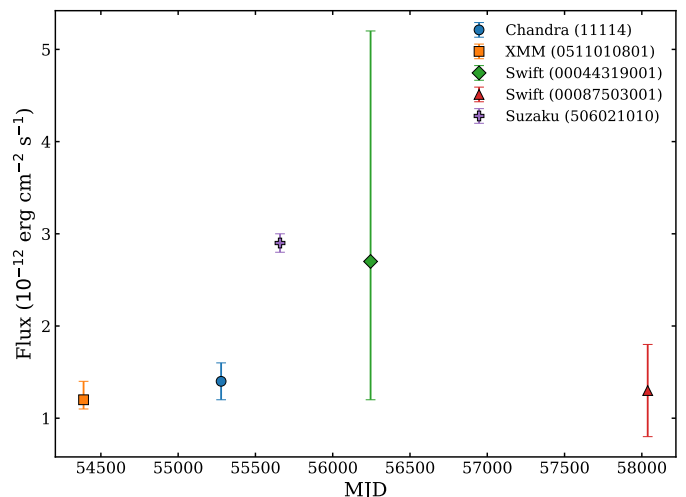


Fig. 4: Long term unabsorbed 2.0–10.0 keV flux variation over time from different observatories, depicting a flux variability in the source.

to be injected with a power-law with exponential cutoff spectrum $dN/dE \propto E^{-\alpha} \exp(-E/E_c)$ with $\alpha = 2$ and $E_c = 50$ TeV, with a minimum energy of $E_{\min} \approx 0.1$ GeV. We further assumed an expected strong and high energy radiation field with temperature $T = 3.5 \times 10^4$ K ($k_B T \sim 3$ eV) and stellar energy density $U \approx 0.1$ erg cm $^{-3}$. The IC upscattering occurs in the deep Klein-Nishina (KN) region in this case. However, we find the IC cooling to be dominant for a magnetic field of $B \sim \sqrt{8\pi f_{\text{KN}} U \frac{F_X}{F_\gamma}} \text{ G} \sim 100$ mG, where f_{KN} is the KN suppression factor, given by $f_{\text{KN}} \approx (1 + (4E \times 2.8 k_B T) / (m_e c^2)^2)^{-1.5} \approx 10^{-3}$ for $k_B T \sim 3$ eV and $E = 1$ TeV (Moderski et al. 2005). The derived set of parameters are similar to that discussed in Hinton et al. (2009) for HESS J0632+057, and that subsequently used for HESS J1832–093 (Eger et al. 2016; Martí-Devesa & Reimer 2020). Assuming an association with SNR G23.11+0.18, which likely resulted from the explosion that created the compact object in the binary, we consider the same age of $t_{\text{age}} \approx 10^4$ yrs and distance of $d \approx 4.6$ kpc as that of the SNR (Maxted et al. 2019). Finally, to explain the SED, the required luminosity in electrons is $L_e \approx 6.5 \times 10^{34}$ erg s $^{-1}$, which is comparable to that obtained by Hinton et al. (2009) for HESS J0632+057, and is compatible with the available kinetic power of the Be-star wind (Waters et al. 1987). As can be seen from Fig. 5, the resulting X-ray and gamma-ray model emission can satisfactorily explain the broadband SED. Note that the model can not explain the GeV data, as the GeV and TeV data can not be explained by a single power-law. This phenomenology is also very typical of gamma-ray binaries, and has been explained using a separate population of leptons accelerated by Coriolis turnover, as a result of orbital motion (Zabalza et al. 2013). Under the inferred spectral parameters, the source should be detectable by the Cherenkov Telescope Array (CTA), making it a promising target for future deep observations aimed at resolving spectral variability and morphology at TeV energies.

Maxted et al. (2019) have previously proposed that HESS J1832–085 TeV emission could arise from the spatially coincident SNR G23.11+0.18 interacting with nearby molecular cloud (MC). This is not unlike HESS J1832–093, where SNR G22.7–0.2 was initially classified as the responsible HE emitter (Acero et al. 2016). Later H. E. S. S. Collaboration

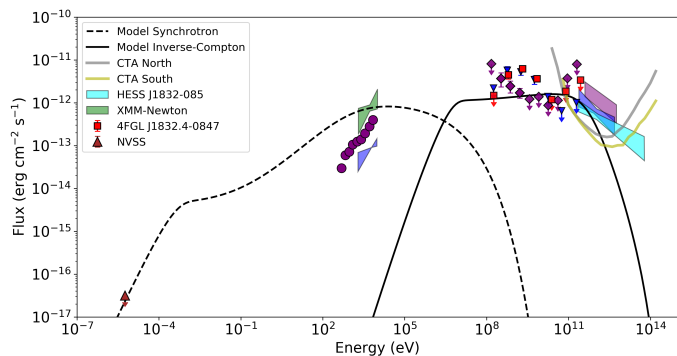


Fig. 5: Broadband SED of HESS J1832–085, along with the model synchrotron and IC emission. The X-ray, GeV, and TeV data for HESS J0632+057 (Hinton et al. 2009; Li et al. 2017) and HESS J1832–093 (Eger et al. 2016; Martí-Devesa & Reimer 2020) are also shown in all purple and all blue, respectively, for comparison.

(2015) argued that the positional offset between SNR G22.7–0.2 and HESS J1832–093, and the presence of infrared and X-ray sources spatially compatible with the gamma-ray emission strongly point against the SNR origin. A similar case can be argued for HESS J1832–085 as well. The moderate positional offset between the H.E.S.S. source and the SNR, the point-like TeV morphology, the presence of a hard non-thermal X-ray source close to the TeV centroid, and indications of its long-term X-ray variability collectively argue against the TeV emission being solely dominated by hadronic processes in an SNR+MC system, and instead favor a compact binary origin. The broadband SED modeling further supports this interpretation, as the observed broadband spectral properties are more naturally explained within a binary scenario. However, a more complex emission scenario cannot be excluded, such as a two-zone structure responsible for the X-ray and TeV emission, or a compact binary component superimposed on a more extended contribution arising from an SNR+MC interaction. A detailed investigation of such hybrid configurations is beyond the scope of this work and is deferred to future studies. We further note that the nearby pulsars, the radio point source, and the IP candidate in the field are unlikely to be physically related to the TeV source, either due to positional offsets, incompatible energetics, or spectral properties that do not match the observed high-energy emission.

Given the limited available data, the archival X-ray observations may have still captured the source during a relatively high flux state, highlighting the need for simultaneous MWL observations to probe X-ray–gamma-ray correlations and constrain variability timescales. Overall, the current MWL evidence favors HESS J1832–085 as a promising gamma-ray binary candidate, with its compact TeV morphology, hard and variable X-ray counterpart, and broadband spectral properties pointing toward a binary origin. Definitive confirmation will require long-term phase-resolved X-ray monitoring to establish orbital modulation, together with deep optical/UV/infrared observations to identify the stellar counterpart and better constrain the non-thermal emission environment.

Acknowledgements. ADS thanks Ömer Faruk Çoban and Guillem Martí-Devesa for helpful discussion regarding *Fermi*-LAT data analysis. ADS is supported by the grant Juan de la Cierva JDC2023-052168-I, funded by MCIU/AEI/10.13039/501100011033 and by the ESF+. This work has been supported by the grant PID2024-155316NB-I00 funded by MICIU /AEI /10.13039/501100011033 / FEDER, UE, and CSIC PIE 202350E189. This work is also partly supported by the Spanish program

Unidad de Excelencia María de Maeztu CEX2020-001058-M, financed by MCIN/AEI/10.13039/501100011033, and by the MaX-CSIC Excellence Award MaX4-SOMMA-ICE, and also supported by MCIN with funding from European Union NextGeneration EU (PRTR-C17.I1).

References

- Abdollahi, S., Acero, F., Ackermann, M., et al. 2020, *ApJS*, 247, 33
- Acero, F., Ackermann, M., Ajello, M., et al. 2016, *ApJS*, 224, 8
- Aharonian, F., Akhperjanian, A. G., Aye, K.-M., et al. 2005, *A&A*, 442, 1
- Aktekin, E. 2025, *Advances in Space Research*, 75, 7751
- Atwood, W., Albert, A., Baldini, L., et al. 2013, arXiv e-prints, arXiv:1303.3514
- Ballet, J., Bruel, P., Burnett, T. H., Lott, B., & The Fermi-LAT collaboration. 2023, arXiv e-prints, arXiv:2307.12546
- Bogovalov, S. V., Khangulyan, D. V., Koldoba, A. V., Ustyugova, G. V., & Aharonian, F. A. 2008, *Monthly Notices of the Royal Astronomical Society*, 387, 63
- Bosch-Ramon & Paredes. 2004, *Astronomy & Astrophysics*, 417, 1075
- Bosch-Ramon, V., Barkov, M. V., Khangulyan, D., & Perucho, M. 2012, *Astronomy & Astrophysics*, 544, A59
- Bruel, P., Burnett, T. H., Digel, S. W., et al. 2018, arXiv e-prints, arXiv:1810.11394
- Burgay, M., Bailes, M., Bates, S. D., et al. 2013, *MNRAS*, 433, 259
- Clifton, T. R. & Lyne, A. G. 1986, *Nature*, 320, 43
- Condon, J. J., Cotton, W. D., Greisen, E. W., et al. 1998, *AJ*, 115, 1693
- Cordes, J. M. & Lazio, T. J. W. 2002, arXiv e-prints, astro
- De Sarkar, A., Roy, N., Majumdar, P., et al. 2022, *ApJ*, 927, L35
- Dubus, G. 2006, *Astronomy & Astrophysics*, 451, 9
- Dubus, G. 2013, *A&A Rev.*, 21, 64
- Eger, P., Laffon, H., Bordas, P., et al. 2016, *Monthly Notices of the Royal Astronomical Society*, 457, 1753
- Frail, D. A., Cordes, J. M., Hankins, T. H., & Weisberg, J. M. 1991, *ApJ*, 382, 168
- H. E. S. S. Collaboration. 2015, *A&A*, 577, A131
- H. E. S. S. Collaboration. 2018, *A&A*, 612, A1
- Hahn, J. 2015, in *International Cosmic Ray Conference*, Vol. 34, 34th International Cosmic Ray Conference (ICRC2015), 917
- Hahn, J., Romoli, C., & Breuhaus, M. 2022, *GAMERA: Source modeling in gamma astronomy*, *Astrophysics Source Code Library*, record ascl:2203.007
- Hinton, J. A., Skilton, J. L., Funk, S., et al. 2009, *The Astrophysical Journal: Letters*, 690, L101
- Hobbs, G., Lyne, A. G., Kramer, M., Martin, C. E., & Jordan, C. 2004, *MNRAS*, 353, 1311
- Huber, D., Kissmann, R., Reimer, A., & Reimer, O. 2021, *Astronomy & Astrophysics*, 646, A91
- Ivezić, Ž., Connolly, A. J., VanderPlas, J. T., & Gray, A. 2020, *Statistics, Data Mining, and Machine Learning in Astronomy. A Practical Python Guide for the Analysis of Survey Data*, Updated Edition
- Johnston, S. & Galloway, D. 1999, *MNRAS*, 306, L50
- Kaur, R., Wijnands, R., Paul, B., Patruno, A., & Degenaar, N. 2010, *MNRAS*, 402, 2388
- Li, J., Torres, D. F., Cheng, K.-S., et al. 2017, *The Astrophysical Journal*, 846, 169
- Lomb, N. R. 1976, *Ap&SS*, 39, 447
- Lyne, A. G., Stappers, B. W., Keith, M. J., et al. 2015, *Monthly Notices of the Royal Astronomical Society*, 451, 581
- Maraschi, L. & Treves, A. 1981, *Monthly Notices of the Royal Astronomical Society*, 194, 1P
- Martí-Devesa, G. & Reimer, O. 2020, *Astronomy & Astrophysics*, 637, A23
- Maxted, N. I., Filipović, M. D., Hurley-Walker, N., et al. 2019, *ApJ*, 885, 129
- Moderski, R., Sikora, M., Coppi, P. S., & Aharonian, F. 2005, *MNRAS*, 363, 954
- Romero, Torres, D. F., Kaufman Bernadó, M. M., & Mirabel, I. F. 2003, *Astronomy & Astrophysics*, 410, L1
- Scargle, J. D. 1982, *ApJ*, 263, 835
- Sironi, L. & Spitkovsky, A. 2011, *The Astrophysical Journal*, 741, 39
- Tam, P.-H. T., Lee, K. K., Cui, Y., et al. 2020, *The Astrophysical Journal*, 899, 75
- VanderPlas, J., Connolly, A. J., Ivezić, Z., & Gray, A. 2012, in *Proceedings of Conference on Intelligent Data Understanding (CIDU)*, 47–54
- Verner, D. A., Ferland, G. J., Korista, K. T., & Yakovlev, D. G. 1996, *ApJ*, 465, 487
- Waters, L. B. F. M., Cote, J., & Lamers, H. J. G. L. M. 1987, *A&A*, 185, 206
- Wilms, J., Allen, A., & McCray, R. 2000, *ApJ*, 542, 914
- Wood, M., Caputo, R., Charles, E., et al. 2017, in *International Cosmic Ray Conference*, Vol. 301, 35th International Cosmic Ray Conference (ICRC2017), 824
- Zabalza, V., Bosch-Ramon, V., Aharonian, F., & Khangulyan, D. 2013, *A&A*, 551, A17

Appendix A: *Fermi*-LAT data analysis

We analyzed ~ 17.3 yr of *Fermi*-LAT P8R3 SOURCE class data (evclass=128, evtype=3; Atwood et al. 2013; Bruel et al. 2018) collected between 2008 August 4 (Mission Elapsed Time (MET) 239557417) and 2025 December 13 (MET 787295981) in the 0.1–500 GeV energy range. The analysis was performed with Fermipy v1.4.0 (Wood et al. 2017), using the P8R3_SOURCE_V3 instrument response functions. Events with zenith angles $> 105^\circ$ were excluded, and the Galactic and isotropic diffuse backgrounds were modeled with gll_iem_v07.fits and iso_P8R3_SOURCE_V3_v1.txt, respectively. All sources from the 4FGL-DR4 catalog (Abdollahi et al. 2020; Ballet et al. 2023) were included in the initial model. A 20° radius region of interest (ROI) centered on HESS J1832–085 was analyzed using a binned likelihood approach over a $15^\circ \times 15^\circ$ region, with 0.1° spatial binning and 8 energy bins per decade. The baseline model was optimized and sources with test statistic (TS) ≤ 25 were removed from the analysis. The normalizations of the diffuse components and of all catalog sources within 3° of HESS J1832–085 centroid were freed and left to vary, while more distant sources were fixed. A search for unmodeled excesses was performed using Fermipy’s source-finding algorithm (TS > 16 , minimum separation 0.2°), followed by a global refit, repeating the above procedure. The final model was used to derive the SED, extension, and localization of the source.

To search for periodicity, the probability of photons coming from 4FGL J1832.4–0847 within a radius of 1° was calculated and assigned using gtsrcprob in Fermi tools. To do this, we adopted the best-fit spectral and spatial models derived from the likelihood analysis. Event weighted gamma-ray light curve was produced assuming a 1-day bin, where each time bin was exposure corrected. Subsequently, we searched for periodicity using the Lomb-Scargle algorithm (Lomb 1976; Scargle 1982) with the AstroML package (VanderPlas et al. 2012; Ivezić et al. 2020) between 1 and 500 days. The bootstrapping statistical method was applied to calculate 1% and 5% significance levels, determined by 10^4 bootstrap resamplings.

Appendix B: X-ray data analysis

Here, we discuss the primary data analysis methodologies for three different instruments. The observation IDs are marked in Fig. 4.

XMM-Newton: The standard data analysis pipelines epproc and emproc for pn and MOS are utilized, and the events are corrected for the background flaring using the espfilt task. The spectra are generated using the evselect tool with filters PATTERN ≤ 4 for pn and PATTERN ≤ 12 and FLAG $=0$ for all CCDs. The energy response matrix and ancillary files are generated using rmfgen and arfgen tasks. The spectra are grouped to a minimum 20 counts per bin and an oversampling factor of 3 using specgroup. The source and background regions are selected using $30''$ radius circles on the same chip.

Chandra: The standard chandra_repro task is utilized to obtain the reprocessed event file, and then spectra from source and background are extracted from $40''$ radius circles using speextract. Such a large extraction region is required because the source in that observation (ID - 11114) is very far off-axis, resulting in a broadened point spread function (PSF). The spectra are grouped until the number of counts in each group exceeds 1, and while spectral fitting, C statistic has been used.

Swift: With a straightforward extraction of data using the xrtpipeline tool, we obtained the event files, and further extracted the spectra from a $30''$ circle for the source, and a $60''$ circle for the background region. The spectra are grouped to 1 count per bin, and while spectral fitting, C statistic has been used. We find that, for both observations, the spectral parameters are consistent with those from the *XMM-Newton* data, but with significantly larger uncertainties due to low statistics. Therefore, we fix the absorption and power-law index parameters to the best-fit value from *XMM-Newton*, to better constrain the flux.